Ionospheric TEC and plasma anomalies possibly associated with the 14 July 2019 M_w7.2 Indonesia Laiwui earthquake, from analysis of GPS and CSES data

YuanZheng Wen[1,2], Dan Tao[1,2]*, GuangXue Wang[1,2], JiaYi Zong[1,2], JinBin Cao[3], Roberto Battiston[4,5], ZhiMa ZeRen[6], and XuHui Shen[6]

[1]Key Laboratory of Earth Exploration and Information Techniques of Ministry of Education, Chengdu University of Technology, Chengdu 610059, China;

[2]School of Geophysics, Chengdu University of Technology, Chengdu 610059, China;

[3]School of Space and Environment, Beihang University, Beijing 100191, China;

[4]Dipartimento di Fisica, Università di Trento, Trento 38123, Italy;

[5]Trento Institute for Fundamental Physics and Applications (TIFPA), National Institute for Nuclear Physics (INFN), Trento 34136, Italy;

[6]National Institute of Natural Hazards, Ministry of Emergency Management of China, Beijing 100085, China

Key Points:
- Ionospheric anomalies in total electron content (TEC) were observed by GPS before a strong earthquake.
- CSES observed ionospheric anomalies in plasma parameters around the earthquake region simultaneously.
- Ionospheric anomalies found in this study are possibly associated the 14 July 2019 M_w7.2 Indonesia Laiwui earthquake.

Abstract: This study presents signatures of seismo-ionospheric perturbations possibly related to the 14 July 2019 M_w7.2 Laiwui earthquake, detected by a cross-validation analysis of total electron content (TEC) data of the global ionospheric map (GIM) from GPS and plasma parameter data recorded by the China Seismo-Electromagnetic Satellite (CSES). After separating pre-seismic ionospheric phenomena from the ionospheric disturbances due to the magnetospheric and solar activities, we have identified three positive temporal anomalies, around the epicenter, at 1 day, 3 days and 8 days before the earthquake (14 July 2019), along with a negative anomaly 6 days after the earthquake. These results agree well with the TEC spatial variations in latitude–longitude–time (LLT) maps. To confirm these anomalies further, we employed the moving mean method (MMM) to analyze ionospheric plasma parameters (electron, O^+ and He^+ densities) recorded by the Langmuir probe (LAP) and Plasma Analyzer Package (PAP) onboard the CSES. The analysis detected on, on Day Two, Day Four, and Day Seven before the earthquake, remarkable enhancements along the orbits around when in proximity to the epicenter. To make the investigations still more convincing, we compared the orbits on which anomalous readings were recorded to their corresponding four nearest revisiting orbits; the comparison did indeed indicate the existence of plasma parameter anomalies that appear to be associated with the Laiwui earthquake. All these results illustrate that the unusual ionospheric perturbations detected through GPS and CSES data are possibly associated with the M_w7.2 Laiwui earthquake, which suggests that at least some earthquakes may be predicted by alertness to pre-seismic ionospheric anomalies over regions known to be at seismic risk. This case study also contributes additional information of value to our understanding of lithosphere–atmosphere–ionosphere coupling.

Keywords: seismo-ionospheric perturbations; CSES satellite; ionosphere; earthquake

1. Introduction

Electromagnetic phenomena possibly associated with natural disasters (earthquakes, tsunamis, and volcanic activities) have been extensively investigated in recent years, of which the seismic-related have been the most important. Although the physical mechanisms responsible for the seismic ionospheric anomalies are still unclear, a significant number of observational studies suggest that there is indeed a connection between the two phenomena. In general, these seismic-related ionospheric disturbances have attracted interest primarily as possible evidence of "earthquake precursors".

To date, two major methods have been used to study seismic-associated ionospheric anomalies: one has analyzed the data collected at the ground-based stations, the other has focused on

data from space-based satellites. The total electron content (TEC) measurement, derived from data collected at local ground-based GPS receivers, was first employed by Liu JY et al. (2001) to study ionospheric electron density variations during the 1999 M_W7.6 ChiChi earthquake; he found that the GPS TEC around the epicenter dramatically decreased in the afternoon period one day, three days, and four days before the earthquake. Later, Liu JY et al. (2004) confirmed the pattern of pre-seismic precursors by statistically investigating the global ionospheric map (GIM) based on data from twenty $M_W ≥ 6.0$ earthquakes in Taiwan from 1999 to 2002; he demonstrated that the local GPS TECs significantly decreased around the epicenter in the afternoon/evening period within five days prior to 16 of the 20 earthquakes. Further investigations of TEC anomalies before strong earthquakes have analyzed GIM data using more reliable statistical methods. For instance, clear precursory positive anomalies of ionospheric TEC were found around the focal region prior to the 2011 M_W9.0 Tohoku-Oki earthquake (Liu JY et al., 2011a; Heki ,2011). Also, Kon et al. (2011) used the superposed epoch analysis (SEA) method to study $M_w ≥ 6.0$ earthquakes that occurred in Japan from 1998 to 2010; they found positive TEC anomalies within 1000 km from the epicenters 1−5 days before the events. One day before the 12 January 2010 M7 Haiti earthquake, the TEC over the epicenter was significantly enhanced. The TECs of the two Mid-latitude dense strips at 35°N and 60°S, and those of seismo-ionospheric anomalies in the ionosphere and plasma density of the epicenter/conjugate point, reached their maximum one day before the earthquake, as the northern crest of the equatorial ionization anomaly (EIA) moved poleward (Liu JY et al., 2011b).

However, in most cases data collected at ground-based stations can be rather limited, because most regions lack an extensive record of ground experiments to monitor geophysical and geochemical parameters. Space-based satellite experiments, with their vast spatial coverage of the seismic areas, therefore can be a more effective way to study seismo-ionospheric effects (Akhoondzadeh et al., 2010). Data from the DEMETER (Detection of ElectroMagnetic Emissions Transmitted from Earthquake Regions) satellite have been employed in many studies, leading to detection of perturbations preceding some strong earthquakes. Anomalies in the O^+ density, ion temperature, electric field, and ELF/VLF/ULF emissions around the epicenter region, detected in DEMETER data, were found (Zhang XM et al., 2009, 2012) to be highly associated with the 12 May 2008 M8.0 Wenchuan earthquake. A statistical study by Akhoondzadeh et al. (2010) reports simultaneous observation of positive and negative anomalies in both DEMETER and GPS data, 1−5 days before all studied earthquakes, under weak and quiet geomagnetic conditions, a result that has been widely regarded as strong evidence of pre-seismic precursors. In addition, examining more than six years of observation data from DEMETER, Zhang XM et al. (2013) found consistent enhancement of electron burst events prior to the seismic activities; in particular, during the entire operation period of the DEMETER satellite. Zeren et al. (2012) found that electron burst precipitation occurred in the ELF/VLF frequency range four days before each strong ($M > 7.0$) earthquake. Using plasma data from DEMETER, Tao D et al. (2017) found that two days before the M7.7 Java earthquake in 2006, both the electron density (N_e) and the

ion density (N_i) increased pronouncedly, the O^+ density increased, the H^+density decreased, and the He^+density remained relatively stable.

Due to the importance and promising prospect of such research into pre-seismic ionospheric anomalies, the China Seismo-Electromagnetic Satellite (CSES) was launched on February 2, 2018 to monitor and study seismo-ionospheric perturbations, and to analyze the features of such perturbations when associated with earthquakes (Shen XH et al., 2018). CSES data have led to some significant results, such as those of Yan R et al. (2018) who studied four $M_w ≥ 7.0$ earthquakes in 2018; their results indicated unusual positive ionospheric perturbations, 1−10 days before the studied earthquakes, in electron density, electron flux, VLF spectrogram, ion density, and ion drift velocity.

Investigations that compare simultaneous observations of multiple physical phenomena, such as the TEC, plasma parameters, and electron and ion motions, can help us better analyze possible relationships between earthquakes and ionospheric disturbances (Zhang XM et al., 2020). Parrot et al. (2006) revealed ionospheric disturbances around the time of strong earthquakes by using measurements of electric field and magnetic field, along with electron and ion data from the DEMETER satellite. Liu J et al. (2016) first combined three altitude techniques to study plasma changes associated with the 2005 M_s7.2 earthquake in Sumatra, Indonesia. They found an unusual enhancement of plasma density around the time of the earthquake by using GPS TEC observations and electron data from the DEMETER satellite at 710 km and N_i records from DMSP satellites at 840 km. Tao D et al. (2017) also found anomalous signatures in plasma density and temperature with data from GPS TEC and DEMETER. With observations from SWARM satellites, the MODIS-Aqua satellite, and from the European Centre for Medium-Range Weather Forecasts (ECMWF), Akhoondzadeh et al. (2018) found potential seismo-ionospheric anomalies in electron density and electron temperature, along with considerable anomalies of the magnetic field, associated with the 16 April 2016 Ecuador M_w7.8 earthquake. A study by Song R et al. (2020) revealed pre-seismic anomalies in electron density and TEC before four $M_W ≥ 5.0$ earthquakes in 2018 by analyzing data from the CSES Langmuir Probe, the IRI-2016 empirical standard model of the ionosphere, and TEC data from the Center for Orbit Determination in Europe (CODE). Zhang XM et al. (2020) also revealed an overlapped electric field possibly associated with the 2018 M_s6.9 Indonesia earthquake, using observations of CSES-VLF transmitter signal perturbations along with the simultaneous anomalous plasma parameters recorded by CSES. All these studies have shown that combining observations of multiple experiments has become a promising approach for advancing Lithosphere–Ionosphere–Atmosphere Coupling (LAIC) mechanism research.

In this study, in order to describe features of seismo-ionospheric anomalies, but also to verify further reliability of new CSES newly scientific observation data, we used cross-validation analysis of GPS TEC data and data from different payload instruments (Langmuir Probe and Plasma Analyzer Package) of CSES to investigate the seismo-ionospheric perturbations associated with the 14 July 2019 M_w7.2 Laiwui earthquake. Basic information about the seismic event and our data sources are briefly introduced in

Section 2. Our methodology and research results are described in Section 3. Section 4 presents discussion and conclusions of this study.

2. Basic Information

2.1 Seismic Event Information

Indonesia is an excellent place to study the phenomenon of seismic–ionospheric anomalies because it is one of the most seismically active regions in the world, with frequent earthquakes. We selected the Indonesian Laiwui earthquake of 14 July 2019 as our research example. The epicenter of the magnitude M_w7.2 earthquake was (0.52°S, 128.17°E) at 10 km depth; it occurred at 09:10 UT (universal time). The radius of the Laiwui earthquake preparation zone estimated by the Dobrovolsky formula $\rho = 10^{0.43M}$ is approximately 1247.38 km (Dobrovolsky et al., 1979).

2.2 GPS Satellite Data

The GPS satellites transmit two L-band signals at the frequencies of 1575.42 and 1227.60 MHz and offer an effective method for monitoring the ionosphere. The TEC is a measure of the total number of electrons that would be contained in a cylinder that extends up vertically above a given point on the Earth all the way through the ionosphere. A network of GPS receivers can be used to monitor the TEC simultaneously and continuously. (Liu JY et al., 2004)

To investigate TEC variations, the GIM data provided by NASA's Jet Propulsion Laboratory (JPL) were adopted to this study. The GIM is constructed into a 5° × 2.5° (Longitude, Latitude) grid with time resolution of two hours. GIM data are generated using data from 150 GPS sites of the IGS and other institutions. In our study, the TEC data are based on the date and geographic location of the Laiwui earthquake from 75 days before to 10 days after (30 April 2019 to 24 July 2019) the main shock.

2.3 China Seismo-Electromagnetic Satellite Data

The China Seismo-Electromagnetic Satellite (CSES), also known as ZhangHeng-1 (ZH-1), was successfully launched on February 2, 2018. The CSES is the first Chinese space-based platform for both earthquake observation and geophysical field measurement. It is a sun-synchronous satellite orbiting at a height of approximately 507 km with a descending node of 14:00 local time (LT), an ascending node time of 02:00 LT, and an inclination of 97.4°. The distance between its neighboring tracks is 2650 km (24° in longitude) in one day, while reduced to 530 km (4° in longitude) in a revisit period of 5 days (Yan R et al., 2018). The main objectives of this mission are to monitor the near-Earth space environment and to investigate possible electromagnetic perturbations related to natural disasters and human activities (Shen XH et al., 2018; Huang JP et al., 2018; Wang Q et al., 2018; Chu W et al., 2018).

The scientific payload of the CSES is composed of several instruments that provide a nearly continuous survey of ionospheric plasma, waves, and energetic particles.

This study makes use of the electron density and electron temperature data derived from the CSES's LAP (Langmuir Probe), and the ion density (He^+, O^+) and ion temperature data derived from its PAP (Plasma Analyzer Package). The CSES completed approximately 100 orbits (most were revisited and overlapped orbits) above the earthquake region between one month before to 10 days after the earthquake (14 June to 24 July, 2019), providing plentiful observation data for our study.

3. Methodology and Research Results

3.1 TEC Anomalies

The moving median and inter-quartile scope of these data are used to shape the upper and lower bounds so that the seismic anomalies could be separated from the background (Liu JY et al., 2004). In addition, to calculate the statistical parameters, the length of the period was selected as about 55 days in order to minimize effects due to seasonal variations. (Richard, 2001; Liu JY et al., 2004; Cai CS, 2007; Liu LB et al., 2009; Liu LB and Chen YD, 2009; Liu LB and Wan WX, 2020; Akhoondzadeh et al., 2010; Olwendo et al., 2012; Elemo et al., 2018). The upper and lower bounds of the mentioned range can be calculated using the following Equations (1)–(4):

$$TEC_{UB} = TEC_{M30} + k \cdot TEC_{IQR}, \tag{1}$$

$$TEC_{LB} = TEC_{M30} - k \cdot TEC_{IQR}, \tag{2}$$

$$\Delta TEC = \frac{(TEC_{obs} - TEC_{M30})}{TEC_{IQR}}, \tag{3}$$

$$p = \pm \left[(\Delta TEC - k)/k \right] \cdot 100\%, \tag{4}$$

where TEC_{M30}, TEC_{IQR}, TEC_{UB}, TEC_{LB}, TEC_{obs}, ΔTEC, k and p are the 30-day TEC moving median value, TEC inter-quartile range, TEC upper bound, TEC lower bound, TEC observed value, differential of TEC, the threshold of the anomaly, and the percentage of TEC change from the undisturbed states, respectively. In this study, we have chosen the anomaly threshold to be $k = 2.0$ based on the magnitude of the main shock. The value k must be dependent on the earthquake magnitude since k increases with earthquake magnitude. For instance, in big seismic events with magnitudes above 7.0, k can be chosen equal to or above 2.0. For our choice of k-value we referred to the methods in the following papers: Akhoondzadeh et al. (Akhoondzadeh et al., 2010; Akhoondzadeh and Saradjian, 2011; Akhoondzadeh, 2012, 2013), Liu JY et al. (2000, 2001, 2004, 2009, 2011a), Tao D et al., (2017), Akpan et al. (2019). When the absolute value of ΔTEC is larger than the k value ($|\Delta TEC| \geqslant k$), the behavior of the pertinent TEC value is considered anomalous.

Basically, we evaluate variations in the geomagnetic data, including variations in Dst, Kp index, and solar flux $F_{10.7}$ index, from 30 May to 24 July 2019, i.e., between 45 days before to 10 days after the M_w7.2 Laiwui earthquake. Furthermore, a strict set of conditions ($Dst > -30$ nT, $Kp < 3$, and $F_{10.7} < 100$ sfu) is adopted to separate pre-seismic ionospheric phenomena triggered by solar and geomagnetic activities from "anomalous" pre-seismic events. Figure 1 shows that solar and geomagnetic activities were relatively weak and quiet during that period except for a magnetic storm that occurred on 10 July 2019, which is marked by red arrows and a dashed ellipse. By a linear interpolation of four data points adjacent to the epicenter (0.52°S, 128.17°E), we calculate the TEC above the epicenter. In consideration of the resolution of GIM TEC
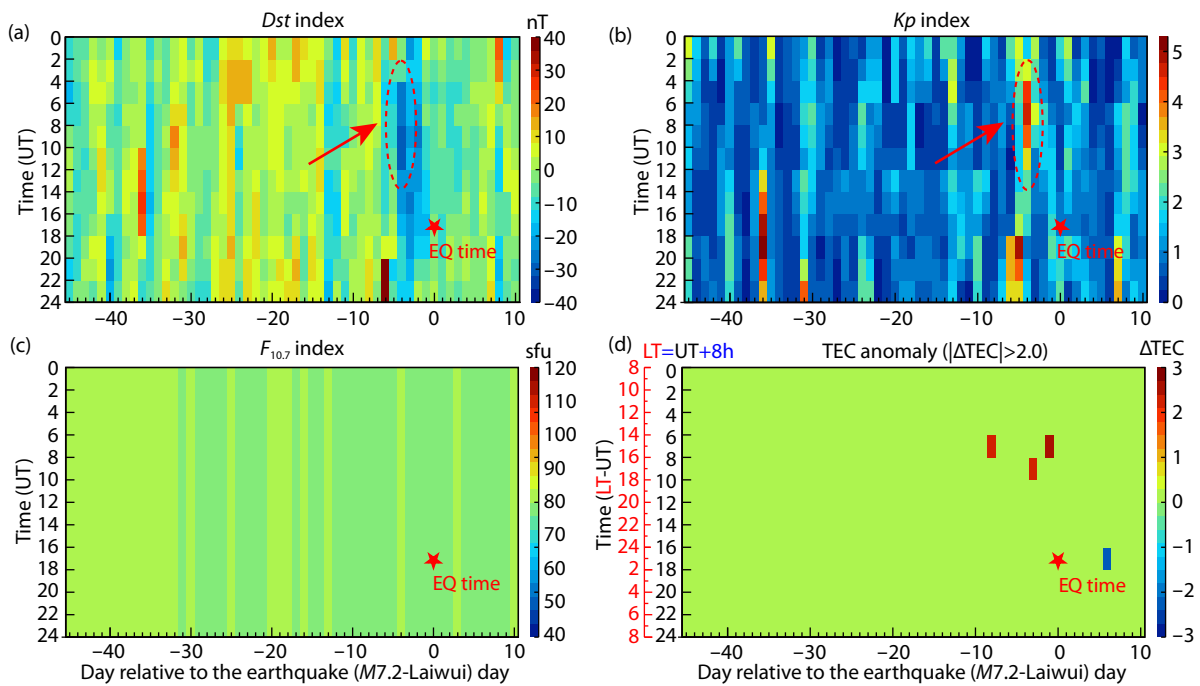
Figure 1. GPS TEC anomaly analysis for the Laiwui earthquake (14 July 2019) from 30 May 2019 (45 days before the earthquake) to 24 July 2019 (10 days after the earthquake). In each display, the earthquake time is represented by a red star; the x axis represents the day relative to the earthquake day; the y axis represents the UT (LT = UT + 8 h). (a) Dst geomagnetic index, and (b) Kp geomagnetic index: duration of the 10 July magnetic storm is marked with the red arrows and dashed ellipses. (c) Solar radio flux $F_{10.7}$ index. (d) Four TEC anomaly durations are marked in red (increased TEC) and blue (decreased TEC). An "anomaly" is defined as $|\Delta TEC| > 2.0$ and the following additional conditions were met: $Dst > -30$ nT, $Kp < 3$, and $F_{10.7} < 100$ sfu. Here 1 TECU $= 10^{16}$ electrons/m^2.

data in latitude and longitude (2.5° in latitude and 5° in longitude), the ranges of 125°–130°E and 0–2.5°S are selected as the data points' center. Figure 1d represents the ΔTEC values between 30 May 2019 and 24 July 2019, according to Equation (3).

In addition, we picked anomalous TEC times by searching for intervals in which $|\Delta TEC| > 2.0$, $Dst > -30$nT, $Kp < 3$, and $F_{10.7} < 100$ sfu. We found such anomalies 8 days (6 July), 3 days (11 July) and 1 day (13 July) before the earthquake and 6 days (20 July) after the earthquake's main shock (marked with a red star, in Figure 1d). Note that the anomalous TEC values were both higher and lower than the median previous TEC, which is consistent with previous research (Akhoondzadeh et al., 2010; Pulinets et al., 2003, 2015; Pulinets and Davidenko, 2014). We find that TEC anomalies, as identified by Equation (4), increased by 22.28% during the interval of 06:00–08:00 UT 6 July (i.e. 14:00–16:00 LT), by 13.85% between 08:00–10:00 UT 11 July (i.e. 17:00–19:00 LT), and by 24.52% between 06:00-08:00 UT 13 July (i.e. 14:00–16:00 LT), but decreased by 22.75% during the interval of 16:00–18:00 UT 20 July (i.e. 00:00–02:00 LT).

3.2 Geographical Anomalies of TEC with Latitude–Longitude–Time (LLT) Maps

Regarding the aforesaid four anomalous time intervals, a geographical investigation checks whether the GIM TEC was disturbed concurrently in each recording locality. Every GIM map consists of 5183 (71 × 73) grid elements, covering ranges of ±87.5°N latitude and ±180°E longitude, with spatial resolution of 2.5° in latitude

and 5° in longitude.

In Figure 2a, the rows "GIM TECs LLT map" are for each of the four anomalous TEC intervals: (06:00–08:00 UT 6 July, 08:00–10:00 UT 11 July, 06:00–08:00 UT 13 July and 16:00–18:00 UT 20 July). For each of the four UT intervals, Figure 2b presents the median (e.g., baseline, reference) value of all TEC measurements at each grid element that were recorded at that location at the same UT time during the 30 days prior to the interval with anomalies. The four rows of Figure 2c present, in chronological order, the ultimate differences ($|\Delta TEC| \geq 2.0$) between each anomalous period of GIM TEC and its preceding-30-day reference value. Generally, the prior-30-day median TEC represents an undisturbed background. A positive TEC difference means that the anomalous GIM TEC was elevated compared to the reference period value; a negative difference means that the anomalous TEC was lower than the median observed in the preceding reference period.

As shown in Figure 2c, the GIM TECs recorded in the zone of the Laiwui earthquake epicenter were dramatically enhanced during the first three anomalous intervals: by ~1.14–31.03% in the 6 July interval, by ~0.75–56.98% in the 11 July interval, and by ~2.75–66.68% in the 13 July interval; and decreased by ~2.70–41.38% in the interval of 16:00–18:00 UT 20 July (00:00–02:00 LT).

To eliminate local time and/or EIA effects, the analysis presented in Figure 2 was repeated, this time using global fixed local time (LT). Figure 3 presents the results. The corresponding extreme enhancements in the GIM TECs, this time recorded at global fixed local times, are again seen to be positioned chiefly around the
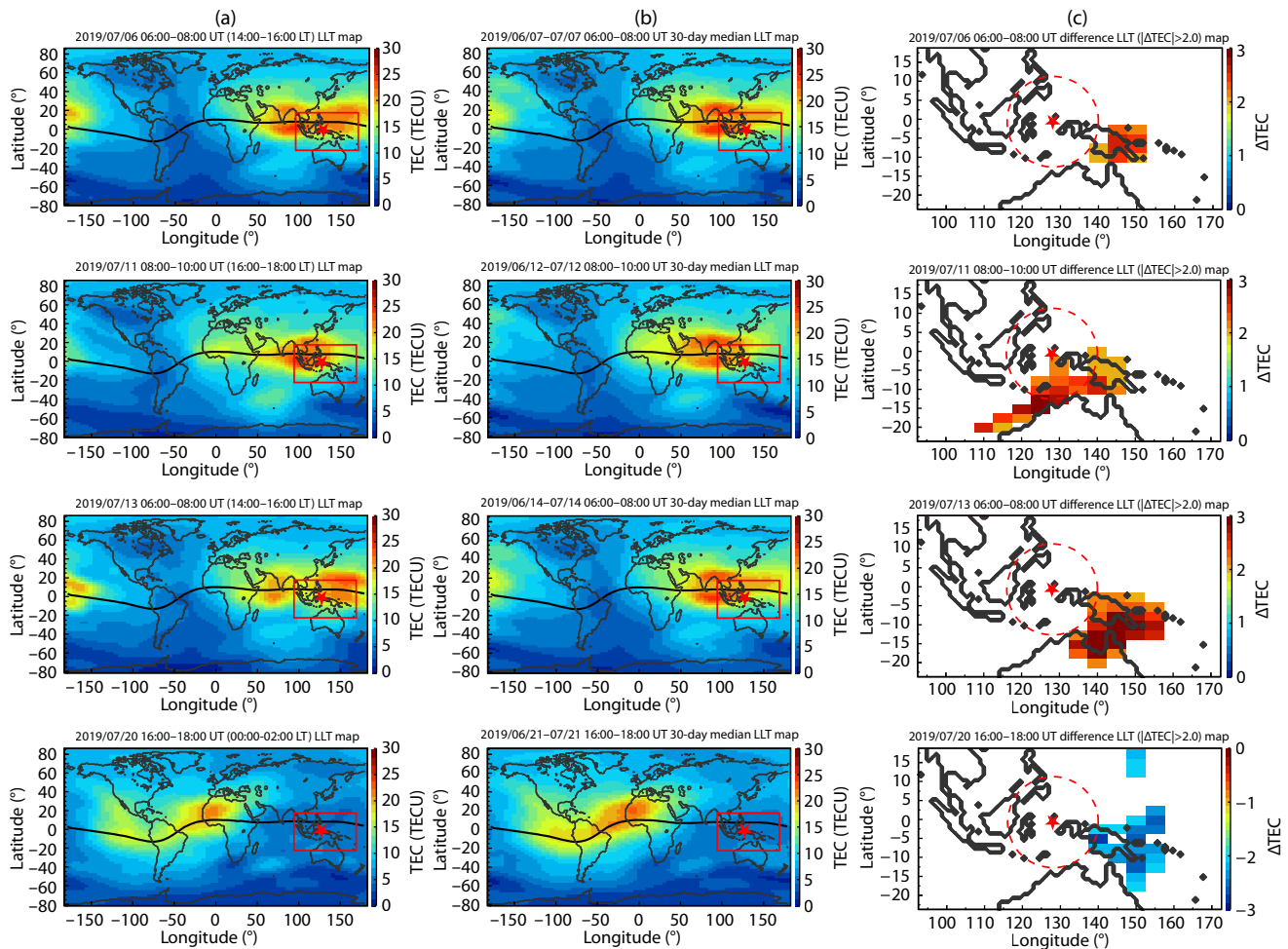
Figure 2. The GIM latitude–longitude–time (LLT) maps of TEC values observed during the four time intervals of anomalous TEC, compared to previous baseline average values: 1st row: 06:00–08:00 UT, 6 July 2019 (8 days before the Laiwui earthquake); 2nd row: 08:00–10:00 UT 11 July (3 days before the earthquake); 3rd row: 06:00-08:00 UT 13 July (1 day before the earthquake), and 4th row: 16:00–18:00 UT 20 July (6 days after the earthquake). Column (a) displays the TEC values, including anomalous values, observed during each of these four intervals. Column (b) presents the median TEC values observed during the same hours of the 30 days before each anomalous interval. The red squares in columns (a) and (b) indicate the region of interest around the earthquake — defined as 22°S–18°N latitude and 95°–170°E longitude. Column (c) displays the times and locations of extreme difference (|ΔTEC| > 2.0) between the anomalous TECs and the corresponding mean TEC values recorded in the 30-day periods prior to the anomalous readings. The colors in column (c) denote the degree of difference between each anomalous TEC and its relevant median value. The red dashed circles (of radius ρ= 1247.38 km) represent what we suggest was this earthquake's "signature area" of the lithosphere, by which we mean the region above which anomalous TEC values were observed before and after the seismic event.

forthcoming epicenter and EIA region. Accordingly, the anomalies simultaneously and remarkably appear geographically in the same four anomalous intervals around the epicenter of the Laiwui earthquake. The GIM TECs around the Laiwui earthquake epicenter are dramatically enhanced, relative to their reference periods, by ~6.98–65.31% in the interval of 06:00–08:00 UT 6 July (14:00–16:00 LT), ~0.45–19.28% in the interval of 08:00–10:00 UT 11 July (16:00–18:00 LT), ~10.00–62.16% in the interval of 06:00–08:00 UT 13 July (14:00–16:00 LT) and decreased by ~5.88–23.53% in the interval of 16:00–18:00 UT 20 July (00:00–02:00 LT). The results of global fixed local time GIM TEC spatial distributions are indeed consistent with the TEC temporal anomalies analysis presented in Subsection 3.1.

3.3 Plasma Parameter Perturbations

GIM TEC anomalies identified in GPS satellite data that were collected 45 days before to 10 days after the earthquake were subjected to cross-validation examination by comparing the TEC observations to observations of plasma parameters made by instruments aboard the CSES.

As introduced in Subsection 2.3, data recorded during the period of 30 days before (14 June 2019) to 5 days after (19 July 2019) the Laiwui earthquake by payloads LAP and PAP on CSES were searched for perturbations of ionospheric plasma parameters above the earthquake preparation zone during that time interval. In particular, we calculated the percentage deviations of the plasma parameters via the moving mean method, using the following equations:
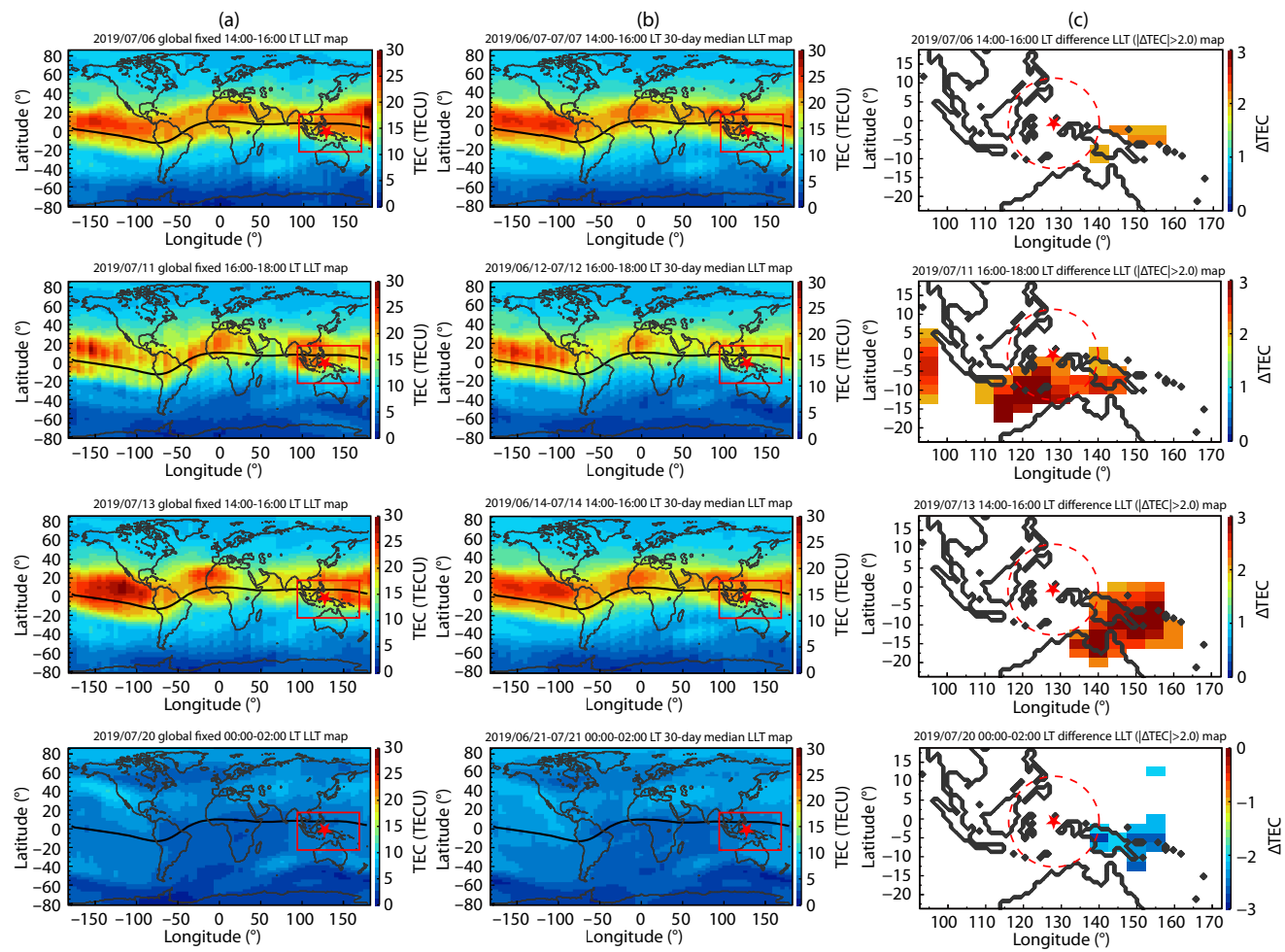
Figure 3.   The GIM LLT maps observed during the *global fixed intervals* (LT) corresponding to those (UT) of Figure 2. All legends are the same as those of Figure 2, except that the time intervals are refined by shifting from UT (universal time) to the more precise LT (local time). Comparison of results in the third columns of Figure 2 and 3 demonstrates that the overall pattern of anomalies is not significantly changed.

$$dN = \frac{N_{obs} - N_{mean}}{N_{mean}} \times 100\%, \qquad (5)$$

$$dT = \frac{T_{obs} - T_{mean}}{T_{mean}} \times 100\%, \qquad (6)$$

where N_{obs} and T_{obs} are the CSES observed values for each plasma parameter, while N_{mean} and T_{mean} are perceived as the background values, defined as the corresponding moving means from the previous 30 days of orbit data (each data cell is sampled by 4° in latitude and 2° in longitude), and deviation of plasma density and temperature are presented as dN, dT respectively. To be more specific, the average values for each parameter of different orbits were calculated using the data from the 30 days before each orbit's date. Indeed, unusual perturbations in different ionospheric plasma parameters were recorded prior to the 14 July Laiwui earthquake.

Figures 4a–e display, respectively, the percentage deviations of electron density (N_e), electron temperature (T_e), O$^+$ density (N_{O^+}), ion temperature (T_i), and He$^+$ density (N_{He^+}). However, due to the measurement limitations of the PAP instrument, valid data for H$^+$ density above the earthquake area are limited and measurements of He$^+$ density for some orbits are intermittent.

Our analysis detected TEC anomalies at 8 days (6 July), 3 days (11 July) and 1 day (13 July) prior to the earthquake. A further cross-validation analysis was conducted on data collected during these periods. As shown in Figure 4a, the electron density increased significantly 4 days (10 July) and 2 days (12 July) before the earthquake, the maximum value increasing by approximately 135% and 116% respectively, as the measurement location approached the epicenter. By comparison, 3 days (11 July) and 1 day (13 July) before the earthquake, the maximum increased by only about 17% and 40%. Similarly, as shown in Figure 4c, the main component O$^+$ density also increased dramatically near the epicenter on 4 days (10 July) and 2 days (12 July) before the seismic event, the maximum values rising by 160% and 154% respectively; however, 3 days before and 1 day before the O$^+$ density remained relatively stable with only slight increases of about 11% and 22%. Although the observation dataset of He$^+$ density is incomplete for some orbits, Figure 4e shows that the tendency of He$^+$ density to vary can still be observed from the data recorded by the CSES. He$^+$ density profoundly increased when the satellite was flying above the epicenter 4 days before the earthquake, by as much as approximately 155%. Electron and ion temperature measurements, however, were relatively stable during the observation
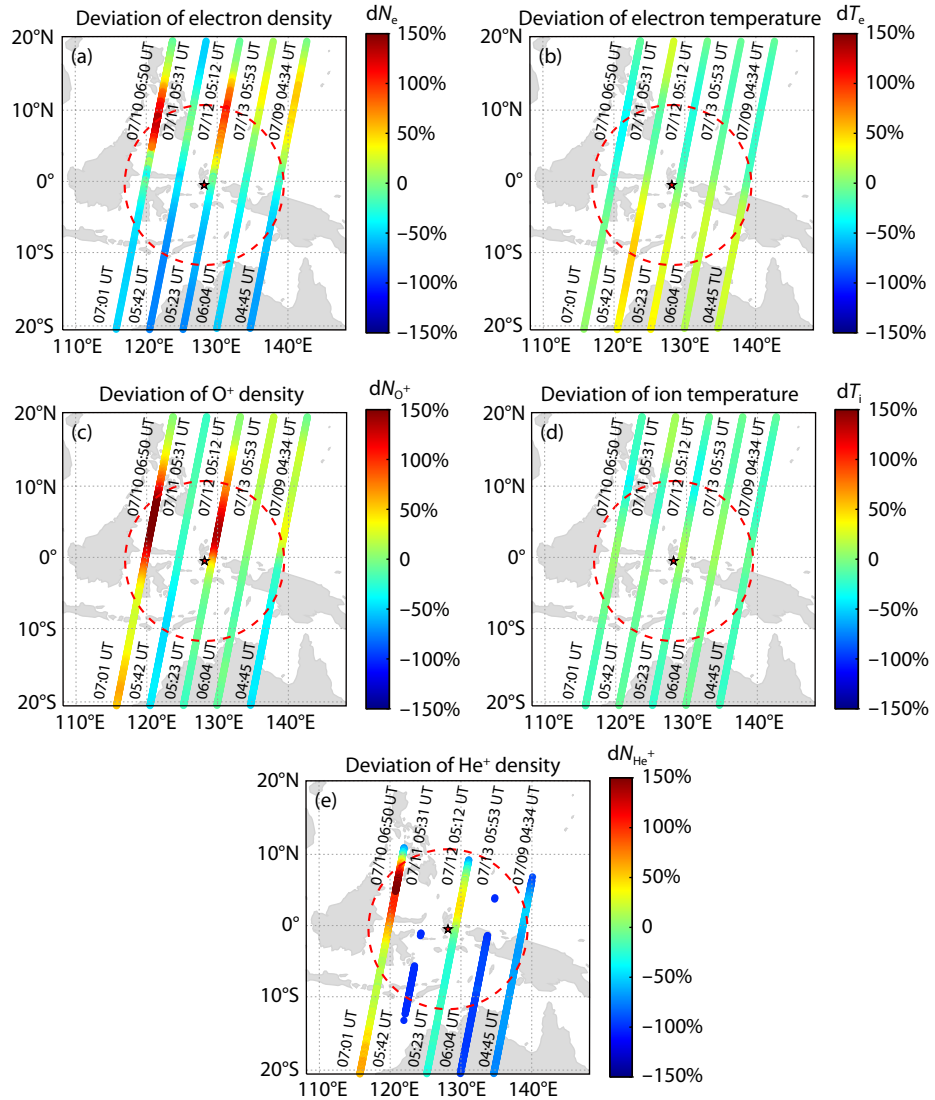
Figure 4.   Deviation percentage of plasma parameters from 9 July to 13 July. The red stars represent the epicenter of the earthquake; the red dashed circles represent the preparation zone (ρ = 1247.38 km) above which anomalous TEC measurements were detected; the precise moments (universal time) of satellite observations above this area are marked at the beginning and end of each orbit.

period, with comparatively slight increases — no more than 60% in temperature for all orbits.

Also, Figures 5a–e display the percentage deviations of the same plasma parameters, but for the observation period from 4 July to 8 July. Since a magnetic storm occurred on 10 July, as shown in Figure 1, it is difficult to distinguish whether the anomalies on 10 July were caused by the magnetic storm or by pre-earthquake events. Figure 5a reveals that the electron density above the region of the epicenter increased dramatically on 5 July and 7 July, the maximum increases reaching approximately 129% and 151%, respectively; the electron densities on 4 July and 6 July, however, remained relatively stable, the greatest deviation percentage reaching no more than 80%. O$^+$ density increased significantly, by 113% and 198% on 5 July and 7 July, while measurements in adjacent orbits remained relatively stable. He$^+$ density increased simultaneously with O$^+$ density on 7 July, the maximum increase reaching around 186%. Furthermore, variations of the electron and ion temperatures remained relatively stable (deviations of no

more than 50%); that is, no significant perturbations were detected during the observation period.

To verify the unusual variations of the in-situ parameters further, electron density (N_e) and electron temperature (T_e) data observed during the orbits yielding anomalous values were extracted and compared to data from their corresponding revisited orbits. Figures 6a and 6b represent the variations of electron density on 12 July and 10 July along with values recorded on their corresponding revisited orbits. It can clearly be observed that the electron density increased significantly above the region 0°–20°N, with a peak value reaching 9.21×10^{10} electrons/m^3 and 9.59×10^{10} electrons/m^3 on 12 July and 10 July, respectively. Although all electron density values increased near the magnetic equator due to the equatorial ionospheric anomaly (EIA), it remains clear that the identified orbits did indeed record unusual positive anomalies, compared to their corresponding revisited orbits. Figures 6c and 6d demonstrate changes of electron tem-
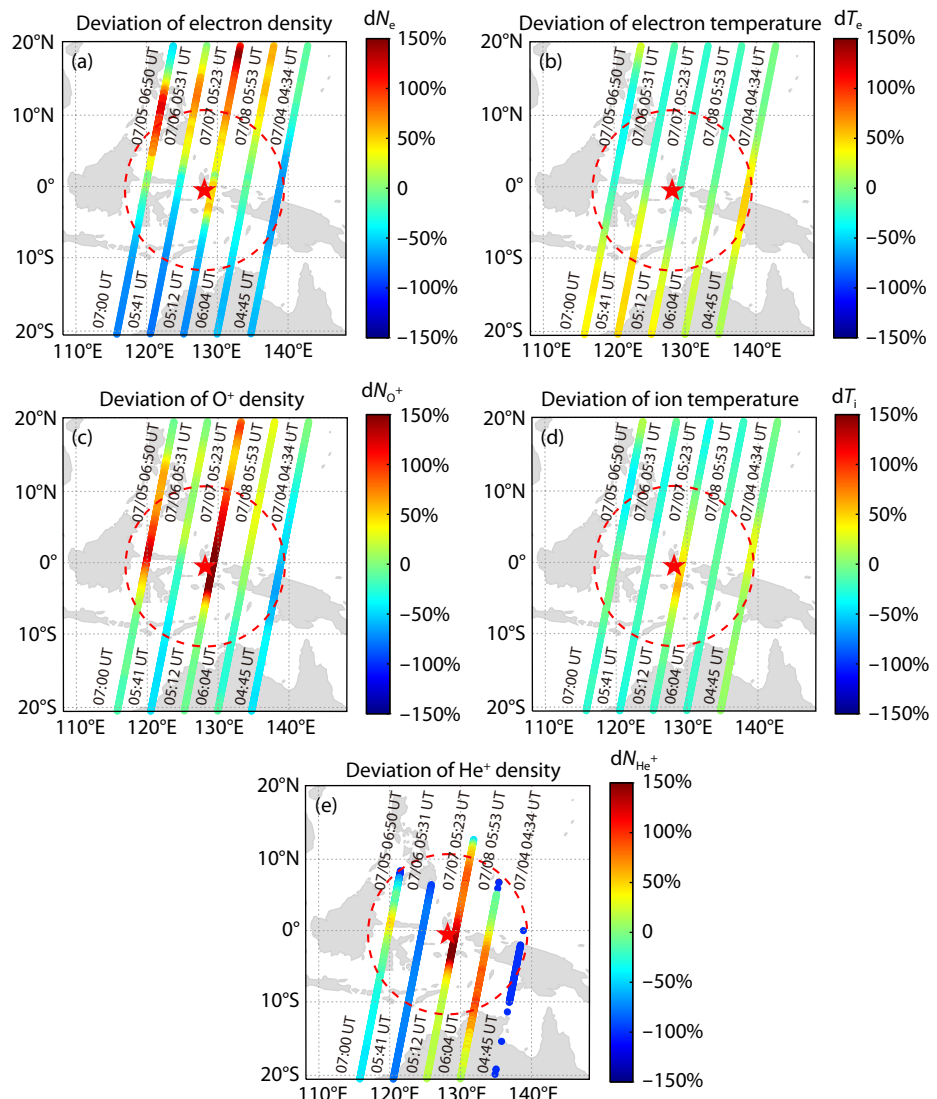
Figure 5. Deviation percentage of plasma parameters from 4 July to 8 July. The red stars represent the epicenter of the earthquake; the red dashed circles represent the preparation zone (ρ = 1247.38 km). The precise moments (in universal time) of the satellite's arrival above this area are marked at the beginning and end of each orbit.

perature recorded on the same orbits; it can be seen that T_e is inversely proportional to N_e. This phenomenon is caused by the cooling process of electrons, of which the rate is proportional to the square of N_e and consistent with basic ionospheric theory concerning the relationship between these two parameters. (Bilitza, 1975; Bilitza and Hoegy, 1990; Kakinami et al., 2011; Song R et al., 2020)

Furthermore, it also should be noted that the CSES usually flew above the earthquake preparation zone twice a day, one orbit descending, the other orbit, ascending. The obviously anomalous disturbances were recorded when the CSES was flying above the region on descending orbits. However, we do not find any similar variations in plasma parameters before the occurrence of earthquake during ascending orbits at about 17:00 UT (02:00 LT).

4. Discussion and Conclusion

This study has focused comprehensively on seismo-ionospheric

anomalies possibly associated with the July 2019 M_w7.2 Laiwui earthquake. Using GPS satellite data, we detected three significant positive perturbations in TEC, at 1, 3, and 8 days prior to the earthquake, and a negative disturbance 6 days after the earthquake under relatively quiet geomagnetic conditions. Taking into consideration local time and EIA effects, the spatial distribution and the signs of the anomalies observed are in good agreement with those of the GPS TEC anomalies (Figure 1d) on each day. Making the results more convincing, more extended types of investigations were carried out, such as in-situ investigations of plasma parameter variations, using data from LAP and PAP instruments aboard the CSES. The results of all these investigations indicate possible seismo-ionospheric anomalies prior to the Laiwui earthquake. It should be noted that some or all of the unusual TEC perturbations on 7 July may have been associated with the M_w6.9 earthquake on that day in Kota Ternate, its epicenter near (0.513°N, 126.19°E) near the epicenter.
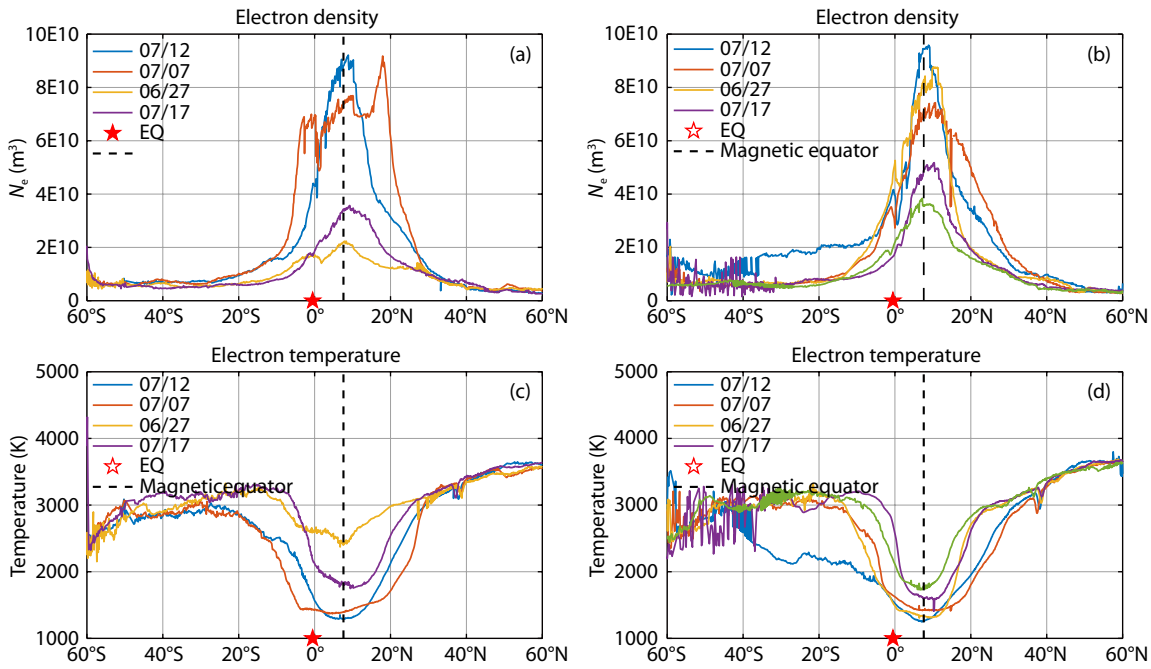
Figure 6. Anomalous variations in N_e and T_e detected in certain orbits, compared to measurements during subsequent orbits that revisit these orbits. Red stars represent the earthquake epicenter; the black dotted line in each subfigure represents the magnetic equator.

Nevertheless, some of the results invite further discussion. A cross-validation analysis of ionospheric anomalies was conducted using the data from GPS TEC and the LAP and PAP instrument aboard the CSES. Its results are consistent with previously-reported ones. We found great enhancements in plasma parameters (electron density, ion density, etc.) prior to the earthquake. However, we note a difference. For example, the most significant anomalies of the electron density were observed on day 4 (10 July) and day 2 (12 July) before the earthquake, while the TEC anomalies were observed exactly one day after the CSES observations. Besides, a negative anomaly in TEC was detected 6 days after the earthquake, but no similar disturbance was detected by CSES instruments. Several reasons could account for these discrepancies: on one hand, as shown in Figure 3b, the Kp index increased between 4:00 and 10:00 UT on 10 July, and the electron density increased simultaneously, so the disturbances on 10 July may be related to geomagnetic activity; on the other hand, the discrepancies may be attributed primarily to differences between the two datasets. To be specific, the CSES is a spacecraft exploring the topside ionosphere at an altitude about 507 km with in-situ observations, while the GPS-TEC is calculated under the assumption of a single layer ionosphere (Song R et al., 2020).

Besides, TEC anomalies were observed outside, as well as within, the putative earthquake preparation zone, as shown in Figure 2 and Figure 3. This can be attributed to the Lithosphere–Ionosphere–Atmosphere Coupling (LAIC) process: the Dobrovolsky formula is an ideal equation that does not consider a LAIC process and makes no distinction among types of epicenter territory location (Song R et al., 2020). Specifically, the seismo-ionospheric anomalies induced by the LAIC mechanism are complicated; its wave channels consist primarily of geochemical (Pulinets et al., 2014), electromagnetic emission (EME) (Hayakawa et al., 2006; Kuo CL et al.,

2011), and acoustic-gravity wave (AGW) propagation (Pulinets, 2004; Pulinets and Boyarchuk, 2004), etc. For this reason, putative earthquake-related TEC anomalies may propagate to greater distances and thus could be observed outside the estimated preparation zone.

As for the observation discrepancies between different CSES orbits (ascending vs. descending ones), the explanation may be the ionospheric daily variation. The descending orbits of the CSES usually flew above the earthquake region at about 15:00 LT (06:00 UT), while the ascending orbits passed there at about 02:00 LT (17:00 UT). The daytime ionosphere receives much more solar radiation, resulting in more ionized particles, significantly increasing the densities of ionospheric electrons and ions, which are much lower at night time. Low densities make variations of ionospheric plasma parameters much more difficult for CSES instruments to detect. Thus, the plasma parameters observed by CSES will appear to remain relatively stable during nighttime measurements, even prior to an earthquake. Also, CSES observations have revealed that perturbations in electron density occur more often than those of electron temperature, which suggests that electron density is much more sensitive to seismic activity than electron temperature (consistent with the conclusions of Liu J et al., 2014). Besides, it should be noted that the PAP instrument of the CSES is slightly contaminated, delivering lower absolute recording values; therefore data from the PAP can currently be used only in relative deviation analysis.

In conclusion, during the periods of anomalous TEC that we have identified, the measurements of GPS TEC and CSES display similar patterns; the temporal and spatial anomalies of the TEC and ionospheric plasma perturbations detected by CSES instruments above the earthquake epicenter did indicate significant positive seismo-ionospheric anomalies. Based on the results presented, we

can also draw the conclusion that CSES data are a reliable input for future studies of seismic events. Also, the localization and synchronization of the anomalies days before the occurrence of this earthquake suggest that these perturbations were possibly associated with the M_W7.2 Laiwui earthquake, but further investigations are required to obtain a more accurate knowledge of the perturbation process and to improve our understanding of the LAIC mechanism.

Availability of Data and Materials
OMNI and GPS data are available from https://cdaweb.gsfc.nasa.gov/sp_phys/. CSES data are accessible from http://www.leos.ac.cn. All earthquake data are available from https: //earthquake.usgs.gov/earthquakes.

Competing Interests
The authors declare that they have no competing interests.

Acknowledgements

References
Akhoondzadeh, M., Parrot, M., and Saradjian, M. R. (2010). Electron and ion density variations before strong earthquakes (*M*>6.0) using DEMETER and GPS data. *Nat. Hazards Earth Syst. Sci.*, *10*(1), 7–18. https://doi.org/10.5194/nhess-10-7-2010

Akhoondzadeh, M., and Saradjian, M. R. (2011). TEC variations analysis concerning Haiti (January 12, 2010) and Samoa (September 29, 2009) earthquakes. *Adv. Space Res.*, *47*(1), 94–104. https://doi.org/10.1016/j.asr.2010.07.024

Akhoondzadeh, M. (2012). Anomalous TEC variations associated with the powerful Tohoku earthquake of 11 March 2011. *Nat. Hazards Earth Syst. Sci.*, *12*(5), 1453–1462. https://doi.org/10.5194/nhess-12-1453-2012

Akhoondzadeh, M. (2013). A MLP neural network as an investigator of TEC time series to detect seismo-ionospheric anomalies. *Adv. Space Res.*, *51*(11), 2048–2057. https://doi.org/10.1016/j.asr.2013.01.012

Akhoondzadeh, M., De Santis, A., Marchetti, D., Piscini, A., and Cianchini, G. (2018). Multi precursors analysis associated with the powerful Ecuador (*M_W*= 7.8) earthquake of 16 April 2016 using Swarm satellites data in conjunction with other multi-platform satellite and ground data. *Adv. Space Res.*, *61*(1), 248–263. https://doi.org/10.1016/j.asr.2017.07.014

Akpan, A. E., Ibanga, J. I., George, N. J., and Ekanem, A. M. (2019). Assessing seismo-ionospheric disturbances using Vanuatu and Honshu earthquakes of March 25, 2007, employing DEMETER and GPS data. *Int. J. Environ. Sci. Technol.*, *16*(11), 7187–7196. https://doi.org/10.1007/s13762-019-02339-x

Bilitza, D. (1975). Models for the relationship between electron density and temperature in the upper ionosphere. *J. Atmos. Terr. Phys.*, *37*(9), 1219–1222. https://doi.org/10.1016/0021-9169(75)90193-2

Bilitza, D., and Hoegy, W. R. (1990). Solar activity variation of ionospheric plasma temperatures. *Adv. Space Res.*, *10*(8), 81–90. https://doi.org/10.1016/0273-1177(90)90190-B

Cai, C. S. (2007). Monitoring seasonal variations of ionospheric TEC using GPS measurements. *Geo-Spat. Inf. Sci.*, *10*(2), 96–99. https://doi.org/10.1007/s11806-007-0034-z

Chu, W., Huang, J. P., Shen, X. H., Wang, P., Li, X. Q., An, Z. H., Xu, Y. B., and Liang, X. H. (2018). Preliminary results of the High Energetic Particle Package onboard the China Seismo-Electromagnetic Satellite. *Earth Planet. Phys.*, *2*(6), 489–498. https://doi.org/10.26464/epp2018047

Dobrovolsky, I. P., Zubkov, S. I., and Miachkin, V. I. (1979). Estimation of the size of earthquake preparation zones. *Pure Appl. Geophys.*, *117*(5), 1025–1044. https://doi.org/10.1007/BF00876083

Elemo, E. O., Ehigiator, M. O., and Ehigiator-Irughe, R. (2018). Seasonal variations of the vertical total electron content (VTEC) of the ionosphere at the GNSS COR station (SEERL) UNIBEN and three other CORS stations in Nigeria. *Niger. J. Technol.*, *37*(2), 286–293. https://doi.org/10.4314/njt.v37i2.1

Hayakawa, M. (2006). Electromagnetic phenomena associated with earthquakes. *IEEJ Transactions on Fundamentals and Materials*, *126*(4), 211–214. https://doi.org/10.1541/ieejfms.126.211

Heki, K. (2011). Ionospheric electron enhancement preceding the 2011 Tohoku-Oki earthquake. *Geophys. Res. Lett.*, *38*(17), L17312. https://doi.org/10.1029/2011GL047908

Huang, J. P., Lei, J. G., Li, S. X., Zeren, Z. M., Li, C., Zhu, X. H., and Yu, W. H. (2018). The Electric Field Detector (EFD) onboard the ZH-1 satellite and first observational results. *Earth Planet. Phys.*, *2*(6), 469–478. https://doi.org/10.26464/epp2018045

Kakinami, Y., Lin, C. H., Liu, J. Y., Kamogawa, M., Watanabe, S., and Parrot, M. (2011). Daytime longitudinal structures of electron density and temperature in the topside ionosphere observed by the Hinotori and DEMETER satellites. *J. Geophys. Res.: Space Phys.*, *116*(A5), A05316. https://doi.org/10.1029/2010JA015632

Kon, S., Nishihashi, M., and Hattori, K. (2011). Ionospheric anomalies possibly associated with *M*≥6.0 earthquakes in the Japan area during 1998–2010: case studies and statistical study. *J. Asian Earth Sci.*, *41*(4-5), 410–420. https://doi.org/10.1016/j.jseaes.2010.10.005

Kuo, C. L., Huba, J. D., Joyce, G., and Lee, L. C. (2011). Ionosphere plasma bubbles and density variations induced by pre-earthquake rock currents and associated surface charges. *J. Geophys. Res.: Space Phys.*, *116*(A10), A10317. https://doi.org/10.1029/2011JA016628

Liu, J., Huang, J. P., and Zhang, X. M. (2014). Ionospheric perturbations in plasma parameters before global strong earthquakes. *Adv. Space Res.*, *53*(5), 776–787. https://doi.org/10.1016/j.asr.2013.12.029

Liu, J., Zhang, X. M., Novikov, V., and Shen, X. H. (2016). Variations of ionospheric plasma at different altitudes before the 2005 Sumatra Indonesia *M_s* 7.2 earthquake. *J. Geophys. Res.: Space Phys.*, *121*(9), 9179–9187. https://doi.org/10.1002/2016JA022758

Liu, J. Y., Chen, Y. I., Pulinets, S. A., Tsai, Y. B., and Chuo, Y. J. (2000). Seismo-ionospheric signatures prior to M≥6.0 Taiwan earthquakes. *Geophys. Res. Lett.*, *27*(19), 3113–3116. https://doi.org/10.1029/2000GL011395

Liu, J. Y., Chen, Y. I., Chuo, Y. J., and Tsai, H. F. (2001). Variations of ionospheric total electron content during the Chi-Chi Earthquake. *Geophys. Res. Lett.*, *28*(7), 1383–1386. https://doi.org/10.1029/2000GL012511

Liu, J. Y., Chuo, Y. J., Shan, S. J., Tsai, Y. B., Chen, Y. I., Pulinets, S. A., and Yu, S. B. (2004). Pre-earthquake ionospheric anomalies registered by continuous GPS TEC measurements. *Ann. Geophys.*, *22*(5), 1585–1593. https://doi.org/10.5194/angeo-22-1585-2004

Liu, J. Y., Chen, Y. I., Chen, C. H., Liu, C. Y., Chen, C. Y., Nishihashi, M., Li, J. Z., Xia, Y. Q., Oyama, K. I., … Lin, C. H. (2009). Seismoionospheric GPS total electron content anomalies observed before the 12 May 2008 *M_w*7.9 Wenchuan earthquake. *J. Geophys. Res.: Space Phys.*, *114*(A4), A04320. https://doi.org/10.1029/2008JA013698

Liu, J. Y., Chen, C. H., Lin, C. H., Tsai, H. F., Chen, C. H., and Kamogawa, M. (2011a).

Ionospheric disturbances triggered by the 11 March 2011 *M*9.0 Tohoku earthquake. *J. Geophys. Res.: Space Phys.*, *116*(A6), A06319. https://doi.org/10.1029/2011JA016761

Liu, J. Y., Le, H., Chen, Y. I., Chen, C. H., Liu, L., Wan, W., Su, Y. Z., Sun, Y. Y., Lin, C. H., and Chen, M. Q. (2011b). Observations and simulations of seismoionospheric GPS total electron content anomalies before the 12 January 2010 *M*7 Haiti earthquake. *J. Geophys. Res.: Space Phys.*, *116*(A4), A04302. https://doi.org/10.1029/2010JA015704

Liu, L. B., and Chen, Y. D. (2009). Statistical analysis of solar activity variations of total electron content derived at Jet Propulsion Laboratory from GPS observations. *J. Geophys. Res.: Space Phys.*, *114*(A10), A10311. https://doi.org/10.1029/2009JA014533

Liu, L. B., and Wan, W. X. (2020). Recent ionospheric investigations in China (2018–2019). *Earth Planet. Phys.*, *4*(3), 179–205. https://doi.org/10.26464/epp2020028

Liu, L. B., Zhao, B. Q., Wan, W. X., Ning, B. Q., Zhang, M. L., and He, M. S. (2009). Seasonal variations of the ionospheric electron densities retrieved from Constellation Observing System for Meteorology, Ionosphere, and Climate mission radio occultation measurements. *J. Geophys. Res.: Space Phys.*, *114*(A2), A02302. https://doi.org/10.1029/2008JA013819

Olwendo, O. J., Baki, P., Mito, C., and Doherty, P. (2012). Characterization of ionospheric GPS Total Electron Content (GPS–TEC) in low latitude zone over the Kenyan region during a very low solar activity phase. *J. Atmos. Sol.-Terr. Phys.*, *84-85*, 52-61. https://doi.org/10.1016/j.jastp.2012.06.003

Parrot, M., Berthelier, J. J., Lebreton, J. P., Sauvaud, J. A., Santolik, O., and Blecki, J. (2006). Examples of unusual ionospheric observations made by the DEMETER satellite over seismic regions. *Phys. Chem. Earth*, *Parts A/B/C*, *31*(4-9), 486-495. https://doi.org/10.1016/j.pce.2006.02.011

Pulinets, S., Legen'ka, A. D., Gaivoronskaya, T. V., and Depuev, V. Kh. (2003). Main phenomenological features of ionospheric precursors of strong earthquakes. *J. Atmos. Sol-Terr. Phy.*, *65*(16-18), 1337–1347. https://doi.org/10.1016/j.jastp.2003.07.011

Pulinets, S. (2004). Ionospheric precursors of earthquakes; recent advances in theory and practical applications. *TAO*, *15*(3), 413–435. https://doi.org/10.3319/TAO.2004.15.3.413(EP)

Pulinets, S.A., Ouzounov, D.P., Karelin, A.V., and Davidenk, D. V. (2015). Physical bases of the generation of short-term earthquake pre-cursors: A complex model of ionization-induced geophysical processes in the lithosphere-atmosphere-ionosphere-magnetosphere system. *Geomagn Aeronomy*, *55*(4), 521–538. https://doi.org/10.1134/S0016793215040131

Pulinets, S., and Boyarchuk, K. (2004). Ionospheric precursors of earthquakes. *Springer Science &Business Media*.

Pulinets, S., and Davidenko, D. (2014). Ionospheric precursors of earthquakes and Global Electric Circuit. *Adv. Space Res.*, *53*(5), 709–723. https://doi.org/10.1016/j.asr.2013.12.035

Richards, P. G. (2001). Seasonal and solar cycle variations of the ionospheric peak electron density: comparison of measurement and models. *J. Geophys. Res.: Space Phys.*, *106*(A7), 12803–12819. https://doi.org/10.1029/2000JA000365

Shen, X. H., Zhang, X. M., Yuan, S. G., Wang, L. W., Cao, J. B., Huang, J. P., Zhu, X. H., Piergiorgio, P., and Dai, J. P. (2018). The state-of-the-art of the China Seismo-Electromagnetic Satellite mission. *Sci. China Technol. Sci.*, *61*(5), 634–642. https://doi.org/10.1007/s11431-018-9242-0

Song, R., Hattori, K., Zhang, X. M., and Sanaka, S. (2020). Seismic-ionospheric effects prior to four earthquakes in Indonesia detected by the China seismo-electromagnetic satellite. *J. Atmos. Sol.-Terr. Phys.*, *205*, 105291. https://doi.org/10.1016/j.jastp.2020.105291

Tao, D., Cao, J. B., Battiston, R., Li, L. Y., Ma, Y. D., Liu, W. L., Zhima, Z. R., Wang, L. W., and Dunlop, M. W. (2017). Seismo-ionospheric anomalies in ionospheric TEC and plasma density before the 17 July 2006 *M*7.7 south of Java earthquake. *Ann. Geophys.*, *35*(3), 589–598. https://doi.org/10.5194/angeo-35-589-2017

Wang, Q., Huang, J. P., Zhang, X. M., Shen, X. M., Yuan, S. G., Zeng, L., and Cao, J. B. (2018). China Seismo-Electromagnetic Satellite search coil magnetometer data and initial results. *Earth Planet. Phys.*, *2*(6), 462–468. https://doi.org/10.26464/epp2018044

Yan, R., Shen, X. H., Huang, J. P., Wang, Q., Chu, W., Liu, D. P., Yang, Y. Y., Lu, H. X., and Xu, S. (2018). Examples of unusual ionospheric observations by the CSES prior to earthquakes. *Earth Planet. Phys.*, *2*(6), 515–526. https://doi.org/10.26464/epp2018050

Zeren, Z. M., Shen, X. H., Zhang, X. M., Cao, J. B., Huang, J. P., Ouyang, X. Y., Liu, J., and Lu, B. Q. (2012). Possible ionospheric electromagnetic perturbations induced by the Ms7.1 Yushu earthquake. *Earth*, *Moon*, *Planets*, *108*(3-4), 231-241. https://doi.org/10.1007/s11038-012-9393-z

Zhang, X. M. (2013). Burst increases of precipitating electrons recorded by the DEMETER satellite before strong earthquakes. *Nat. Hazards Earth Syst. Sci.*, *13*(1), 197–209. https://doi.org/10.5194/nhess-13-197-2013

Zhang, X. M., Chen, H. R., Liu, J., Shen, X. H., Miao, Y. Q., Du, X. B., and Qian, J. D. (2012). Ground-based and satellite DC-ULF electric field anomalies around Wenchuan M8.0 earthquake. *Adv. Space Res.*, *50*(1), 85–95. https://doi.org/10.1016/j.asr.2012.03.018

Zhang, X. M., Qian, J. D., Ouyang, X. Y., Shen, X. H., Cai, J. A., and Zhao, S. F. (2009). Ionospheric electromagnetic perturbations observed on DEMETER satellite before Chile *M*7.9 earthquake. *Earthq. Sci.*, *22*(3), 251–255. https://doi.org/10.1007/s11589-009-0251-7

Zhang, X. M., Wang, Y. L., Boudjada, M. Y., Liu, J., Magnes, W., Zhou, Y. L., and Du, X. H. (2020). Multi-Experiment Observations of ionospheric disturbances as precursory effects of the indonesian Ms6.9 earthquake on August 05, 2018. *Remote Sens.*, *12*(24), 4050. https://doi.org/10.3390/rs12244050 https://doi.org/10.3390/rs12244050

Supplementary Materials for "Ionospheric TEC and plasma anomalies possibly associated with the 14 July 2019 Mw 7.2 Indonesia Laiwui earthquake, from analysis of GPS and CSES data"

The 55 days day to day TEC data are provided as supplementary Figure S1, other CSES orbits with plasma parameter variations are provided as supplementary Figures S2 and S3.
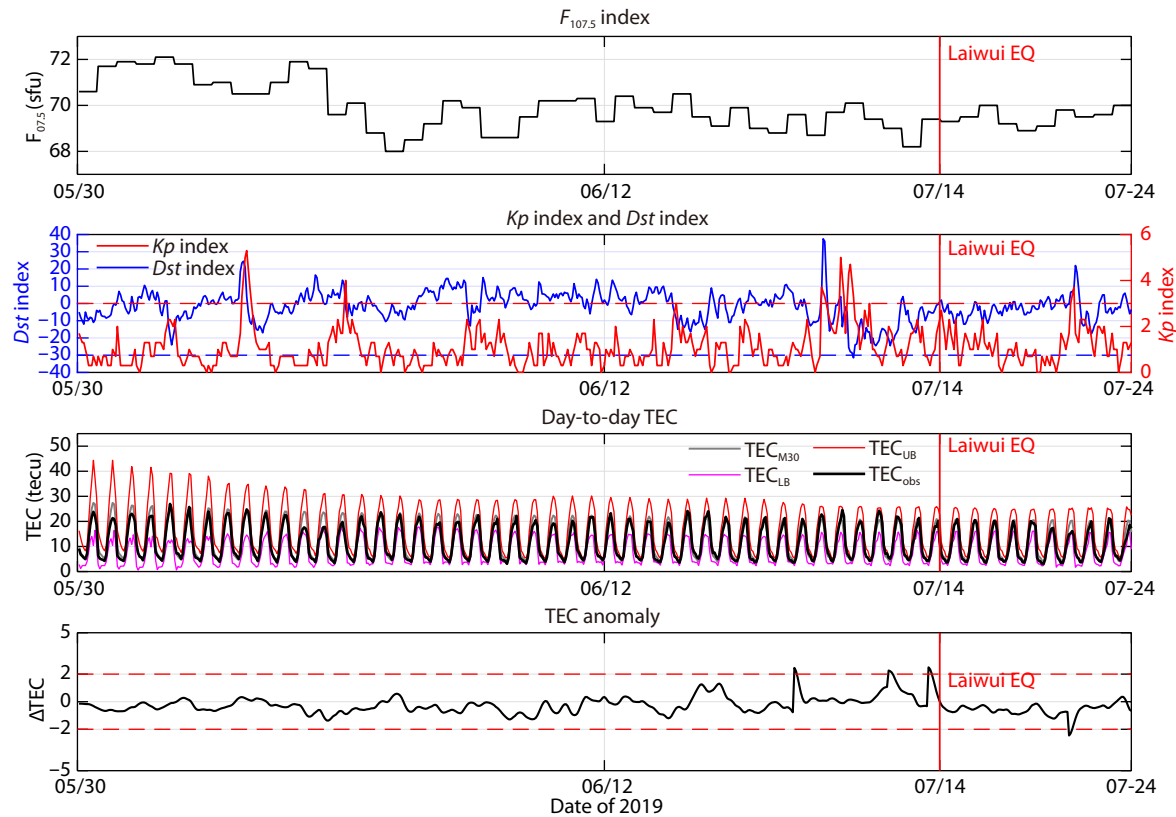

Figure S1. (a) F10.7 index (b) Kp and Dst index (c) Day-to-day TEC data variations and corresponding UB and LB from May 30 2019 to 24 July 2019. (d) Detected TEC anomalies.
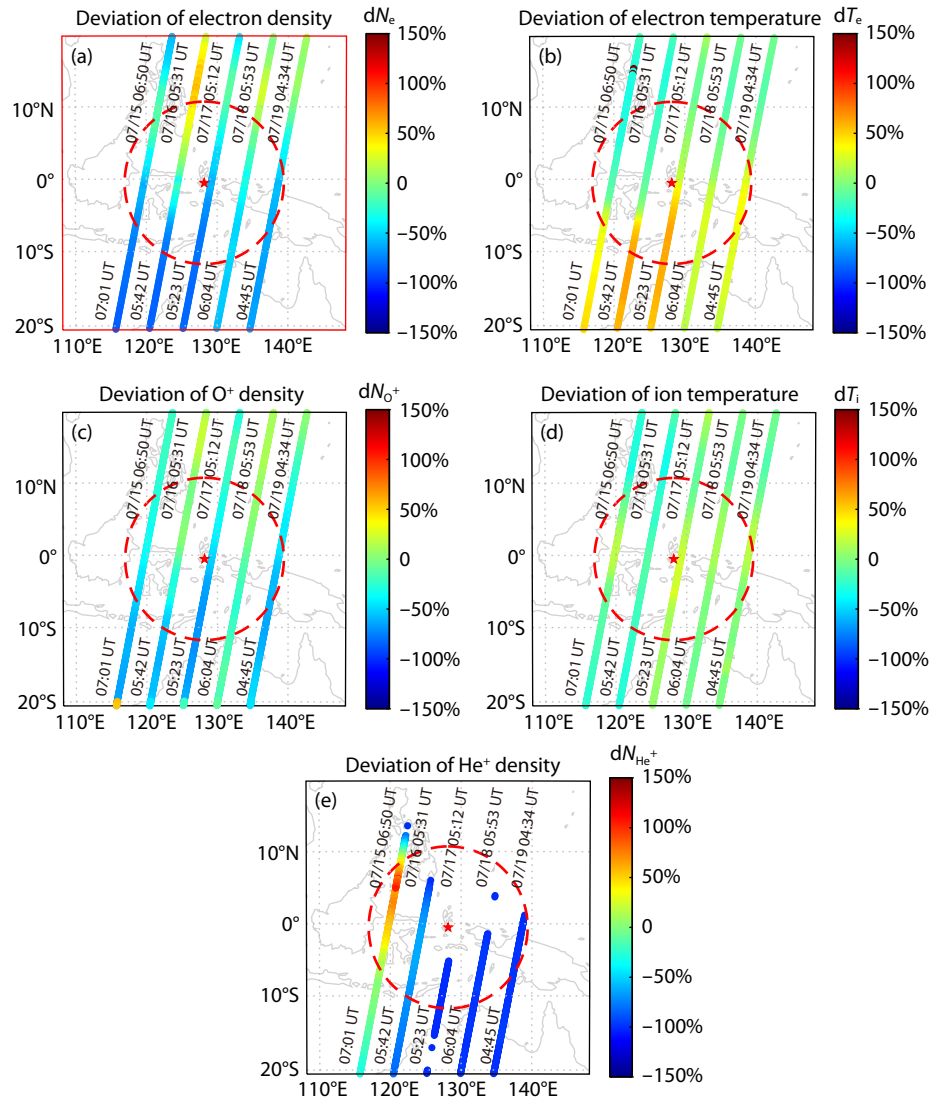
Figure S2. Deviation percentage of plasma parameters from 15 July to 19 July. The red stars represent the epicenter of the earthquake and the red dashed circles represent the preparation zone (ρ=1247.38 km), the precise moments (universal time) of flying above this area are marked at the beginning and end of each orbit.
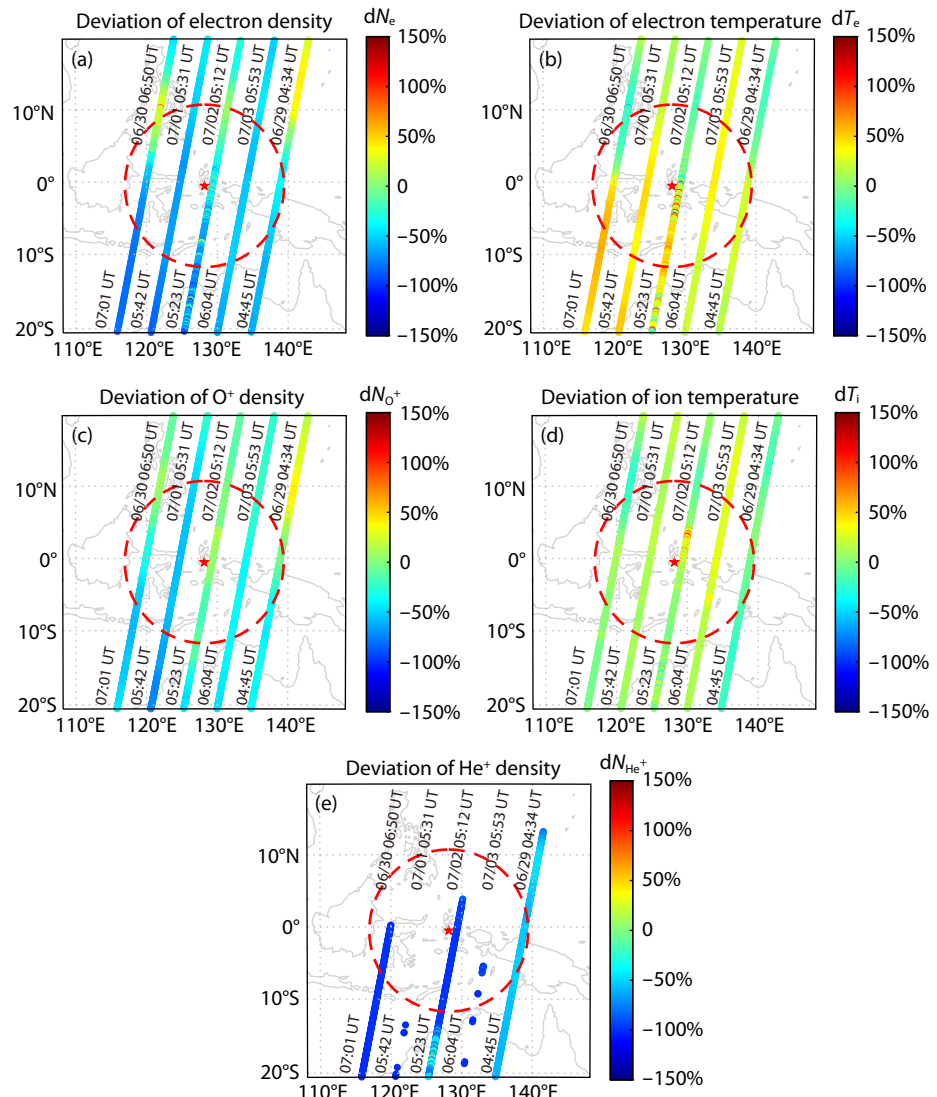
Figure S3. Deviation percentage of plasma parameters from 29 June to 3 July. The red stars represent the epicenter of the earthquake and the red dashed circles represent the preparation zone (ρ=1247.38 km), the precise moments (universal time) of flying above this area are marked at the beginning and end of each orbit.
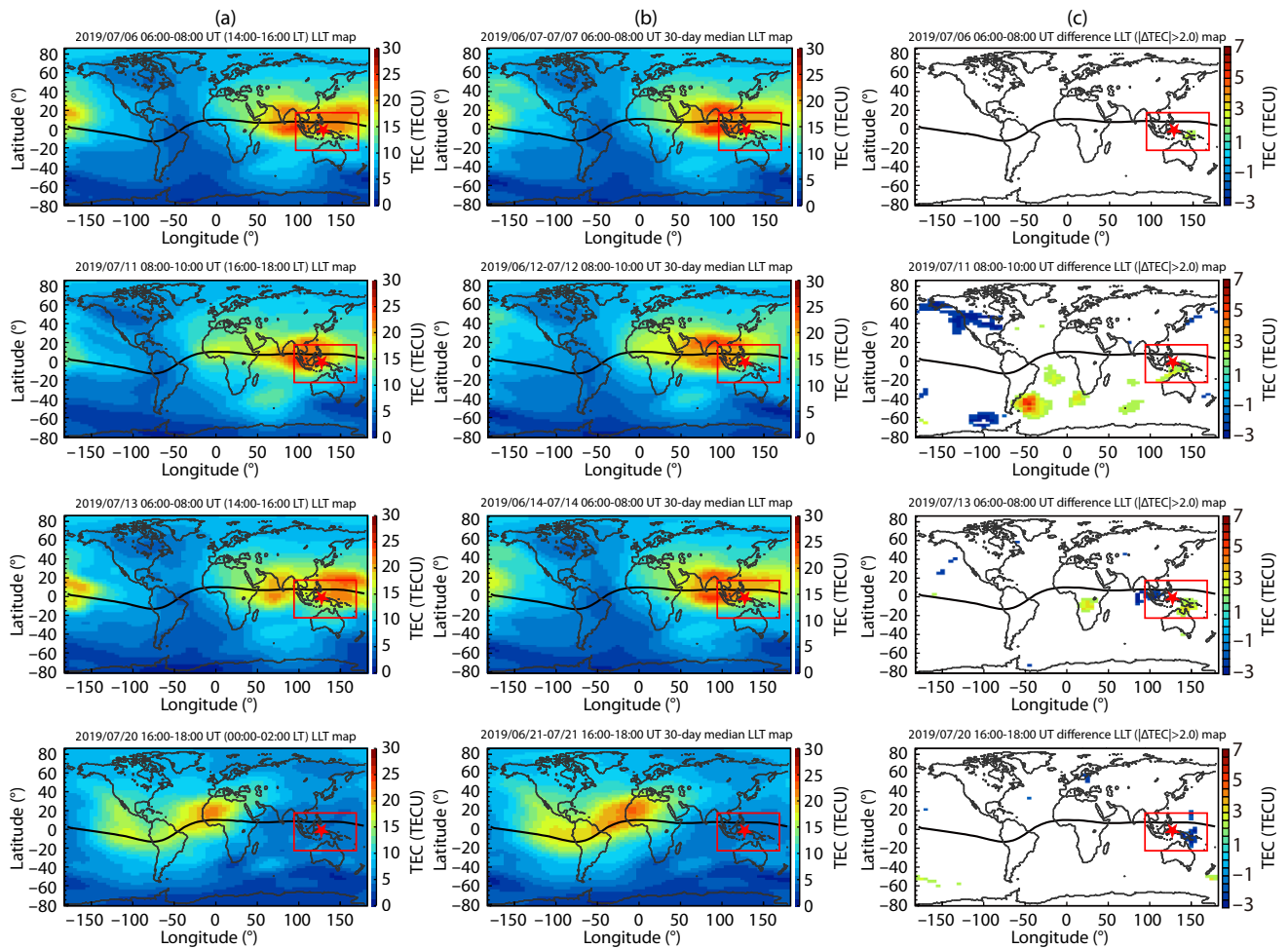
Figure S4. The GIM latitude-longitude-time (LLT) maps observed during the interval of 06:00-08:00 UT 6 July, 08:00−10:00 UT 11 July, 06:00−08:00 13 July before the 14 July 2019 M_W7.2 Laiwui earthquake and 16:00−18:00 UT 20 July after the14 July 2019 M_W7.2 Laiwui earthquake. The GIM LLT maps during the fixed period of 06:00−08:00 UT 6 July 2019 (1st column), 08:00−10:00 UT 11 July 2019 (2nd column), 06:00−08:00 UT 13 July 2019 (3rd column) and 16:00−18:00 UT 20 July 2019 (4th column). Panels of row (a) are the observed values on 8 days before the earthquake (6 July 2019), 3 days before the earthquake (11 July 2019), a day before the earthquake (13 July 2019) and 6 days after the earthquake (20 July 2019), while row (b) shows the median values of the period of days 1–30 before each anomalous interval. Panels of row (c) denote the extreme global scaled differences ($|\Delta TEC| > 2.0$) of the 30-day period that appeared on 8 days before the earthquake (6 July 2019), 3 days before the earthquake (11 July 2019), a day before the earthquake (13 July 2019) and 6 days after the earthquake (20 July 2019). The red rows (a, b, c) indicate the regions of interest around the earthquake, in range of 22°S–18°N latitude and 95°−170°E longitude. Panels of row (d) denote the extreme differences ($|\Delta TEC| > 2.0$) of the 30-day period that appeared on 8 days before the earthquake (6 July 2019), 3 days before the earthquake (11 July 2019), a day before the earthquake (13 July 2019) and 6 days after the earthquake (20 July 2019) with the regions of interest around the earthquake. The color denotes the difference value of the TEC from the relevant median value. The red dashed circles with the radius ρ=1247.38 km represent the earthquake preparation area of the lithosphere. squares in
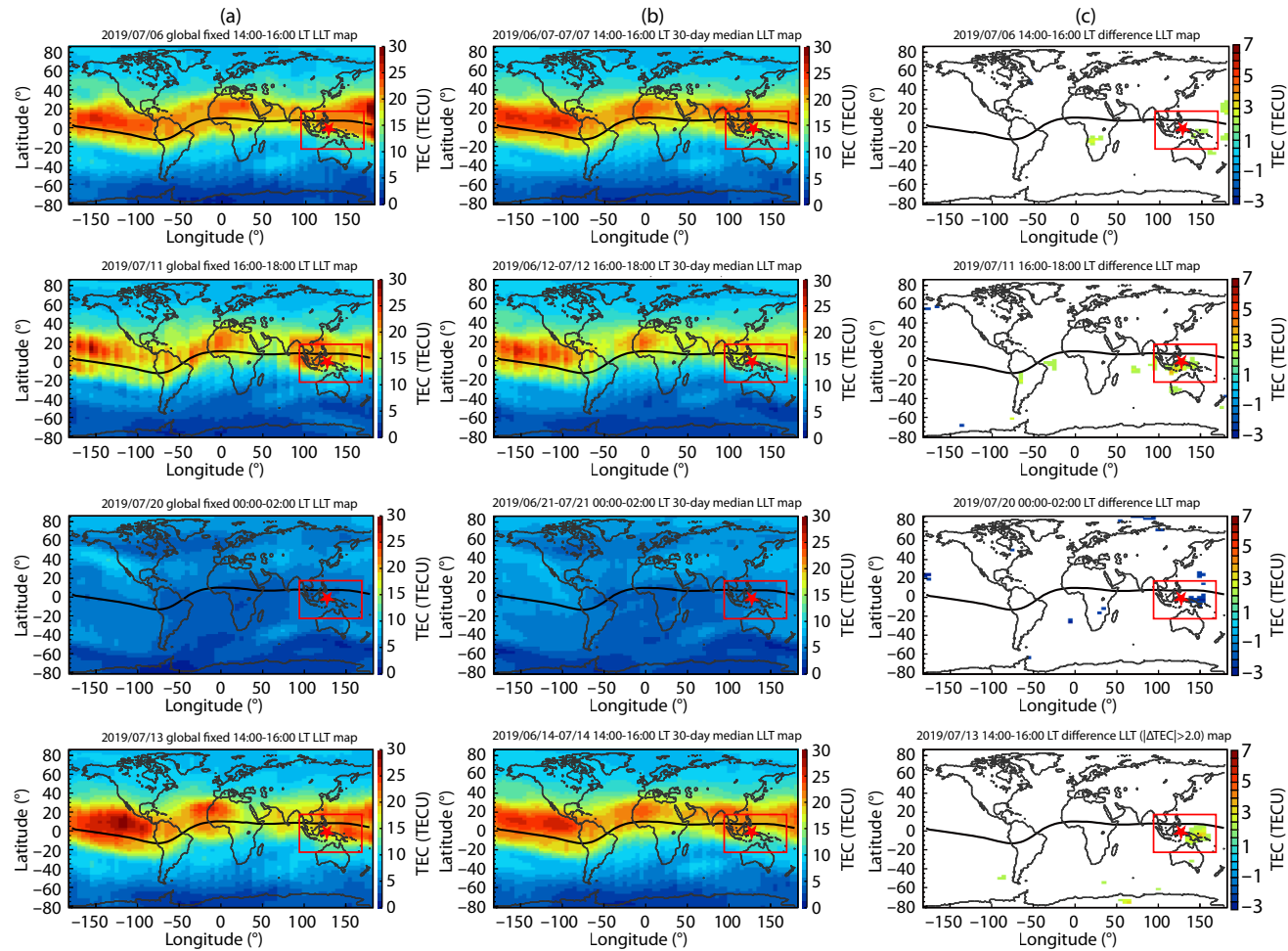
Figure S5. The GIM LLT maps observed during the global fixed intervals of 15:00–17:00 LT 6 July, 17:00–19:00 LT 11 July, 15:00-17:00 LT 13 July before the earthquake and 01:00-03:00 LT 20 July after the earthquake. The GIM LLT maps during four global fixed local times: (1st column) 15:00–17:00 LT 6 July 2019, (2nd column) 17:00-19:00 LT 11 July 2019, (3rd column) 15:00–17:00 LT 13 July 2019 and (4th column) 01:00-03:00 LT 20 July 2019, respectively. Panels of row (a) are the observed values on 8 days before the earthquake (6 July 2019), 3 days before the earthquake (11 July 2019), a day before the earthquake (13 July 2019), and 6 days after the earthquake (20 July 2019), while row (b) shows the median values of the period of days 1–30 before each anomalous interval. Panels of row (c) denote the extreme global scaled differences ($|\Delta TEC| > 2.0$) of the 30-day period that appeared on 8 days before the earthquake (6 July 2019), 3 days before the earthquake (11 July 2019), a day before the earthquake (13 July 2019) and 6 days after the earthquake (20 July 2019). The red squares in rows (a, b, c) indicate the regions of interest around the earthquake, in range of 22°S–18°N latitude and 95°–170°E longitude. Panels of row (d) denote the extreme differences ($|\Delta TEC| > 2.0$) of the 30-day period that appeared on 8 days before the earthquake (6 July 2019), 3 days before the earthquake (11 July 2019), a day before the earthquake (13 July 2019) and 6 days after the earthquake (20 July 2019) with the regions of interest around the earthquake. The color denotes the difference value of the TEC from the relevant median value. The red dashed circles with the radius ρ=1247.38 km represent the earthquake preparation zone.